Journal of Power Technologies 100 (1) (2020) 59–67

# The numerical analysis of the basic operating parameters of a low-NOx burner

Bartłomiej Hernik *, Radosław Brymora †

**Abstract**

More importance than ever before is attached to reducing harmful gas emissions from industry, both in Poland and worldwide. Rising prices of gas emissions allowances, stricter criteria for suitability for use and the desire to protect the environment are driving the search for new technological solutions and logistics to deliver cost savings and lower emissions. The creation of an appropriate numerical model can translate into real savings as well as having other benefits. This paper presents a numerical analysis of the basic operating parameters of a low-emission swirl burner. The analyzed burner is a typical example of a burner with air staging. The burner was placed in a cylindrical combustion chamber. In the first stage, a cold flow analysis without reaction was performed showing the velocity profile, flow vectors and the flow of coal particles. Then calculations were carried out taking into account combustion of coal dust particles in the chamber. The analysis of combustion products, temperatures prevailing in the chamber and the content of nitrogen oxides is presented.

**Keywords**: CFD modelling, low-NOx burner, combustion, coal

## Introduction

Issues relating to reducing harmful gas emissions have now become extremely important in industry, in Poland and elewhere across the globe [1]; [2]; [3]. Rising prices of gas emissions allowances, stricter criteria for suitability for use and the desire to protect the environment are driving the search for new technological solutions and logistics to deliver cost savings and lower emissions. One of the most effective primary methods for cutting nitrogen oxides is technology based on low-NOx swirl burners (LSB). LSB burners largely prevent the formation of nitrogen oxides by using combustion zones and swirling the jets of reactants. LSB burners are characterized by much lower $NO_x$ emissions than conventional burners used in pulverized-fuel boilers. Creating an appropriate numerical model can translate into real savings as well as having side benefits. One obvious advantage of CFD modelling is the relatively low cost compared to experimental calculations. CFD modelling makes it possible to make quick changes to the model without additional financial outlays, set any external conditions of the task, test the model in conditions that might be considered dangerous and make models that are impossible to create experimentally (e.g. due to their very large or very small scale). In [3] syngas swirling flame characteristics obtained by numerical modelling are presented. Modelling of non-premixed swirl burner flows using a Reynolds-stress turbulence closure was shown in [4]. The authors made a comparison between the k–ϵ model and the Reynolds-stress model. Experiments on a rotating-pipe swirl burner were presented in [5]. Laser-Doppler measurements of mean velocity components and Reynolds stresses are performed. The swirling motion is generated by the rotating outer pipe of the annular air passage. In [6] multivariate numerical tests were carried out to lower $NO_x$ emissions in a large scale coal-fired boiler. The results of numerical simulations of particle sticking behavior near the throat of a low-$NO_x$ axial-swirl burner in a 600-$MW_e$ bituminous coal burned boiler are presented in [7]. A comparison of simulation results with measurements using a probe with hot-film sensors shows that the numerical model offers a reasonable description. When fuel is burned in the burner, a burnout is formed. In [8], the pulverized coal flame was examined for ash deposition. In [2] the main objective of the study was to investigate how the results obtained with three radiative heat transfer methods – the P1 approximation method, Discrete transfer and the DO method – fit the temperature field in a boiler furnace on pulverized coal with OFA ports. The results obtained with the DO, DT model give a better fit for the measurements. Predicting radiative transfer in axisymmetric cylindrical enclosures using the Discrete Ordinates Method is presented in [9]. This analysis shows that the predictions are most sensitive to particle number densities and temperatures, while little sensitivity to the absorption and scattering efficiencies is detected. In [10] numerical modeling of a turbulent natural gas flow through a non-premixed industrial burner of a slab reheating furnace

*Politechnika Śląska e-mail
†Politechnika Śląska e-mail

was presented. The main purpose of the numerical investigation is to determine the turbulence model that more consistently reproduces the experimental results of the flow through an industrial non-premixed burner orifice. The main objective of the analysis showed in [11] was to compare the results obtained numerically with results obtained experimentally. Comparing the data measured with those calculated, a satisfactory convergence using the PDF model was achieved. A study of air flow and pulverized coal transport in low-NOx burners was presented in [12]. The measured concentration of the coal dust was compared with the numerically predicted distribution of particles. Both the measurements and the calculations show a highly non-uniform concentration of particles at the burner outlet. Numerical analysis of pulverized coal combustion characteristics using an advanced low-NOx burner was shown in [13]. The results show that a recirculation flow is formed in the high-gas-temperature region near the burner outlet. The residence time of coal particles in this high-temperature region, promotes the evolution of volatile matter and the progress of char reaction, and produces an extremely low-$O_2$ region for effective NO reduction.

## Theory

Nitrogen oxides are formed in the process of combustion of nitrogen compounds contained in fuel (fuel NOx) and nitrogen contained in atmospheric air (thermal NOx). The principle of operation of swirl burners is based on intentional swirling of pulverised-air mixture and air jets. The swirling of the jets causes more precise mixing of the reactants and a higher rate of combustion. On the other hand, it also causes raised emissions of nitrogen oxides. The reduction in nitrogen oxides emissions resulting from combustion of pulverized coal is based on creating combustion zones, each with an appropriately selected excess air factor. The combustion temperature has a direct impact on the amount of NOx compounds created. Therefore, a control mechanism is required. The temperature of combustion may be modified by changing the excess air factor. As the excess air factor becomes smaller, the mixture gets richer in fuel and the combustion temperature becomes lower. This leads to smaller amounts of thermal nitrogen oxides being produced. Two basic types of low-emission swirl burners are used in industry. The principle of operation is based on air staging in the first case and on fuel staging in the second. In the first case, the air of each jet is staged. The combustion zones are distributed uniformly, the dust-air mixture gradually changes from very rich ($\lambda$˜ 0.6) to slightly super-stoichiometric ($\lambda$˜ 1.2). This method is presented schematically in Fig. 1.

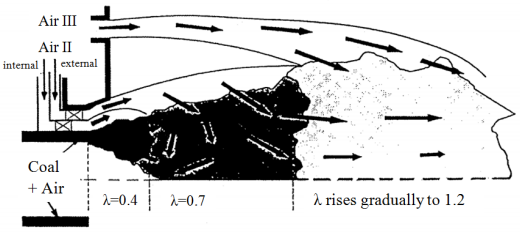


Figure 1: Air staging in a low-emission dust burner [14]

In the second case, the dust-air mixture flows very rapidly through the core and "crosses" the super-stoichiometric mixture causing a drop in temperature. This concept is presented in Fig. 2.

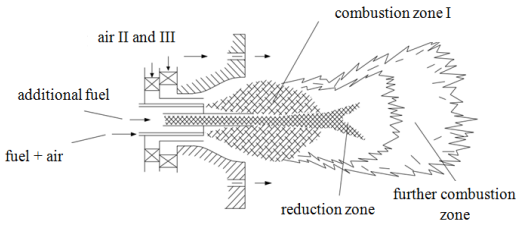


Figure 2: Fuel staging in a low-emission dust burner [14]

## Boundary conditions and modelling description

A model of a low-emission swirl burner is presented below together with a simulation performed using the Ansys Fluent program. The constructed burner model is a typical example of a burner with air staging. The model has three inlets – the air flows through two external inlets and the coal dust mixture flows though the central tunnel. Each stage has swirling vanes and, additionally, each dust-air mixture jet has an extra pre-swirler. The burner is placed in a cylindrical furnace with the following dimensions: radius $r$=2 m and length $L$=6 m. Table 1 presents the vane inclination angle for each jet (where $\alpha$ – angle to the flow axis and $\beta$ – angle to the burner wall). The geometry is presented on Fig. 3. Due to the dimensions, the view with a visible furnace was omitted. Fig. 4 shows a 3D representation of a fluid flow area with the furnace.

Since neither the heat transfer between the walls nor any parameters of the burner envelope material were

Table 1: Inclination angles and number of vanes on subsequent stages of swirlers

| Stage | α° | B° | Number of vanes |
|---|---|---|---|
| Pre-swirler | 15 | 30 | 6 |
| Stage I swirler | 15 | 30 | 6 |
| Stage II swirler | 30 | 45 | 24 |
| Stage III swirler | 45 | 50 | 12 |

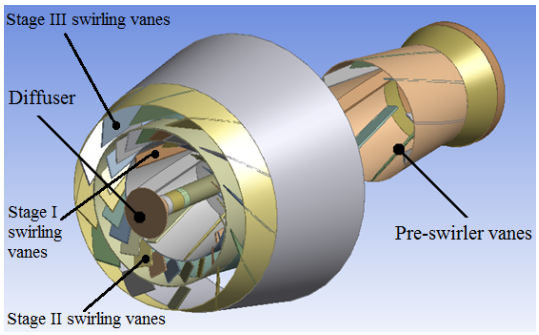


Figure 3: 3D representation of the model of a low-NOx swirl burner

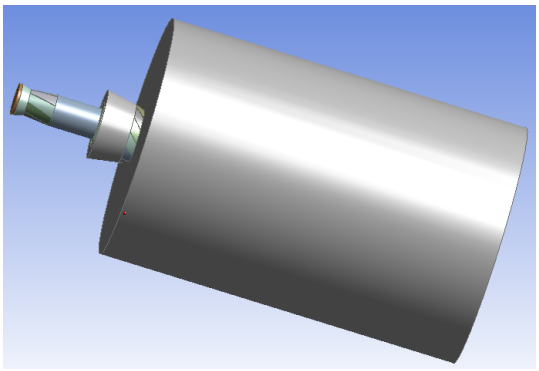

Figure 4: 3D model of the fluid flow area with the furnace

taken into consideration, the mesh was made for the fluid only. It consists of hexahedral and tetrahedral elements (Fig. 5). The latter constitute about 60% of the whole. The furnace (not visible on Fig. 5) is made of hexahedral elements only.

The quality of the elements was assessed using the skewness factor, which determines the similarity of a given cell to an equilateral one; 1 denotes the worst element and 0 an equilateral one. In the created mesh the worst element is characterized by the value of 0.75 which, considering the rather complex geometry, is a satisfactory result. To shorten the computation time, the number of cells is reduced to 711,365; the number of nodes is 117,325.

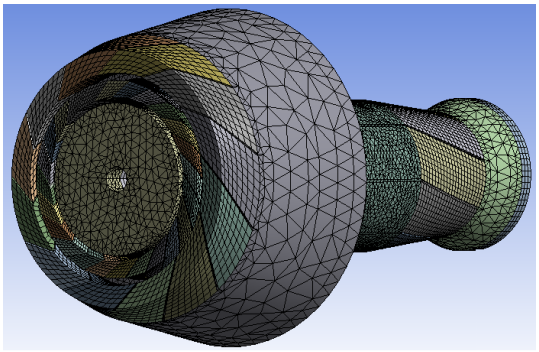

Figure 5: Mesh of the low-NOx swirl burner model

The RANS (Reynolds-Averaged Navier–Stokes) approach is selected in the project due to the universality of the scale modelling and the relatively low computing power required. The $k$-$\varepsilon$ (2 eqn) RNG model was selected for turbulence calculations [12]; [13]. This is the most common model used in industry, because it offers a fair compromise between the speed of computations and the reliability of obtained results. Since the analyzed model is characterized by an eddy flow, the "Swirl Dominated Flow" option was selected. The SIMPLE method was used to estimate the flow fields [13]; [10]. The Euler-Lagrange two-phase approach is more accurate than the Euler-Euler approach in the case of coal combustion modelling. The species transport model was used to simulate the continuous phase. To model the trajectories of the moving fuel particles in flue gas, the Lagrange approach was used [7]; [11]; [12]. It allows a precise setting of the coal grain size. The particle size is adjusted to the Rosin-Rammler distribution standard. And the coal distribution in numerical model is described using the Rosin-Rammler distribution method [12]. The fed fuel particles are assumed to have a spherical shape.

The heat, mass and momentum transfer between the pulverized coal particle and flue gas were computed. Chemical reactions were calculated using the Eddy-Dissipation model [2]; [10]; [11], which assumes infinitely fast reactions. Chemical kinetics are represented by a global reaction (a two-stage reaction in this case). The reaction of the mechanism of the volatile fraction combustion and carbon monoxide oxidization is presented below. Coefficients m, n, l, k, and j were obtained based on the coal composition according to volumetric reactions.

$$C_m H_n O_l N_k S_j + (\frac{m-l}{2} + \frac{n}{4} + j)O_2 \xrightarrow{\text{k1}} mCO + \frac{n}{2}H_2O + \frac{k}{2}N_2 + jSO_2 \quad (1)$$

$$CO + 0.5O_2 \xrightarrow{k2} CO_2 \quad (2)$$

The possibility of modelling coal devolatilization and char combustion is the greatest advantage of the two-phase approach. The reaction of char oxidation to $CO_2$ is presented below.

$$C + O_2 \rightarrow CO_2 \quad (3)$$

The Discrete Ordinates radiation model [1]; [2]; [10] was used to calculate the radiation between the furnace chamber wall and the coal particle surface. The emissivity and exchange of radiation between the flue gases and the particles were also modelled by DO model [10]; [2]; [1]. The gray gas model was used to simulate flue gas absorptivity [10]. The absorptivity is calculated based on the concentration of $CO_2$ and $H_2O$. The concentration of NO was investigated using thermal and fuel nitrogen oxides. The Zeldovich mechanism [15] was used to calculate the formation of thermal nitrogen oxides. As a result of energy supply in the oxygen molecule bonds are broken and free atoms O can react in two equations:

$$N_2 + O \leftrightarrow NO + N \quad (4)$$

$$N + O_2 \leftrightarrow NO + O \quad (5)$$

In conditions similar to stoichiometric conditions and in fuel-rich mixtures, a third reaction was proposed to contribute to the formation of thermal $NO_x$ [16]; [17]; [18]:

$$N + OH \leftrightarrow NO + H \quad (6)$$

The fuel nitrogen is distributed between the volatiles and the char. It was assumed that the fraction of N in the volatiles is converted to HCN and $NH_3$. However, the fraction of N in the char is converted to NO directly. Table 2 presents the numerical model assumptions.

Tables 3, 4 and 5 present the inlet parameters of the jets of air and the dust-air mixture, the hard coal parameters ($R_x$ means residue on x sieve, grain size in the form of the content of grains bigger than x), as well as the coal calorific value and elemental analysis, respectively.

Table 2: Assumptions of the numerical model

| | |
|---|---|
| Two-phase model | Euler- Lagrange [7]; [11]; [12] |
| Turbulence model | RNG k-e [12]; [13] |
| Combustion model | Eddy-Dissipation [3]; [10]; [11] |
| for the coal particle | Flue gas absorptivity: wsggm-domain-based model [10] |
| De-volatilization | Single Rate model [13] |
| Combustion of char | The kinetic-diffusion model [7]; [12] |
| Radiation model | DO [1]; [2]; [10] |
| | Flow Iterations per radiation iteration: 1<br>Theta divisions: 4<br>Phi divisions: 4<br>Theta pixels: 3<br>Phi pixels: 3 |

Table 3: Air and dust-air mixture jets inlet parameters

| Data | Unit | Value |
|---|---|---|
| Air mass flow I | kg/s | 3.91 |
| Coal mass flow | kg/s | 1.17 |
| Air mass flow II | kg/s | 1.29 |
| Air mass flow III | kg/s | 5.05 |
| Mixture temperature | oC/K | 105/378 |
| Secondary air temperature | oC/K | 270/543 |

Table 4: Coal grain size

| x | mm | 88 | 102 | 120 | 150 | 200 |
|---|---|---|---|---|---|---|
| Rx | % | 49.5 | 24.3 | 15.6 | 8.3 | 2.3 |

Table 5: Coal analysis (as-received state)

| Calorific value | Qri | kJ/kg | 22692 |
|---|---|---|---|
| Ash content | Ar | % | 19.2 |
| Moisture content | Wrt | % | 9 |
| Carbon content | Cr | % | 57 |
| Hydrogen content | Hr | % | 4 |
| Sulfur content | Sr | % | 1 |
| Oxygen content | Or | % | 9 |
| Nitrogen content | Nr | % | 0.8 |

# Results

## Reactionless flow analysis

In the flow analysis, as a post-processing result, a number of pictures were obtained characterizing a flow with no reaction. Fig. 6 presents the velocity profile along the YZ plane. The maximum velocity at which air flows through the channel is about 30 m/s, whereas the average velocity for all channels of the burner is approximately 20 m/s. The biggest acceleration values can be observed in the narrowings of the dust-air channels and at the stage outlet of air II. The calculated values are close to those of the Babcock-Energy burner [12]. Therefore, the values obtained numerically may be considered as real.

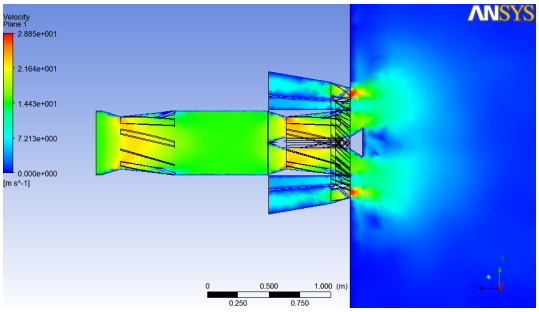


Figure 6: Velocity distribution [m/s] in a swirl burner along the YZ plane

The flow vectors are presented in Fig. 7. A change in the direction of the vectors can be observed at the burner inlet into the furnace. This is the effect of the burner vanes curvature causing a vortex. The last picture related to the reactionless flow analysis presents the flow of only the coal particles injected into the inlet (Fig. 8). It can be seen that a vortex is formed on the flow path of the particles. The velocity of the analyzed coal particles does not exceed 25 m/s, which is a real value.

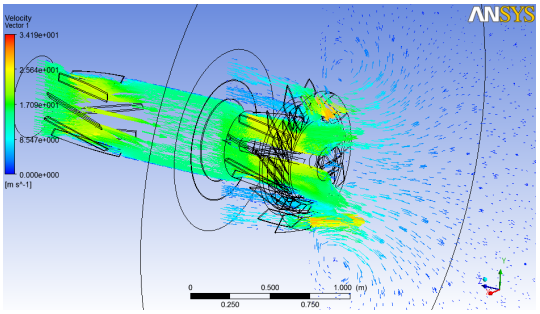


Figure 7: Velocity vectors [m/s] in a swirl burner along the YZ plane – isometric view

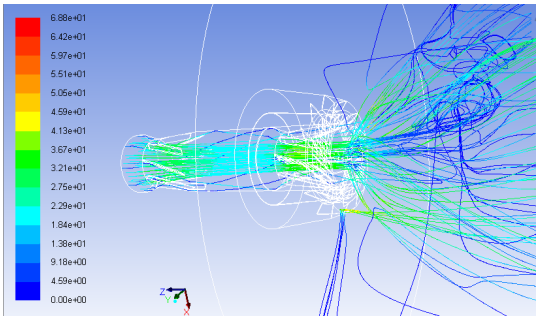


Figure 8: Flow path of coal particles in the burner – colour depending on velocity [m/s]

## Analysis of the flow with reactions

The pictures below present the fluid velocities during combustion. Since no chemical reactions related to combustion take place in the burner itself, the velocity profile in it remains unchanged. Significant changes occur in the furnace – the fluid velocity rises substantially due to the differences in pressures resulting from the combustion process. Analyzing Figs. 9-10, the formation of combustion zones can be noticed. Fig. 9 presents the velocity profile along the YZ plane.

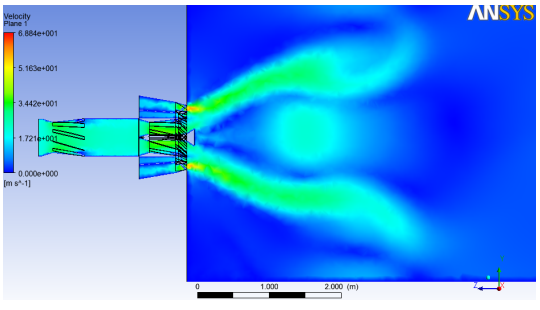


Figure 9: Velocity distribution [m/s] in the burner along the YZ plane – reactions taken into account

The picture below demonstrates the formation of vortices, which is a desirable phenomenon in this type

of burner. The streamlines are colored depending on velocity.

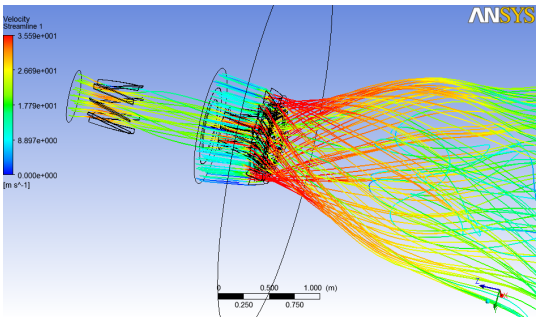


Figure 10: The jet flow path through the burner and through the furnace – path color depending on velocity [m/s]

One of the more essential parts of CFD modelling is the analysis of combustion products and furnace temperatures. Since by assumption the model created was constructed as a burner with air staging, some characteristic features of this burner type can be found in it. The first step leading to a comparative analysis is the distribution of temperature and the forming zones preliminarily discussed in the previous section. The temperature distribution obtained during the combustion process in the set furnace is presented on Fig. 11. The maximum temperature reached was approximately 2500 K, which is the temperature of the flame itself. The value seems slightly inflated due to the type of model of turbulent combustion applied. This inflated temperature value results from the fact that the model ignores free radicals and dissociation effects. A similar phenomenon can be observed in [11], where a rise in temperature compared to measured temperature values is shown. Undesirable though it may be, this phenomenon is characteristic of this type of model. Another essential feature resulting from Fig. 11 is the flame shape, which is typical of dust swirl burners – the flame is moved away from the burner outlet, and combustion zones can be noticed where a drop in temperature occurs between the flame and the furnace walls. The drop is caused by air supplied to the burner from inlet II ( Fig. 3). The flame location itself indicates that $\lambda$ is close to one in that region (due to the highest temperature). Therefore, it may be stated that the model and the results obtained satisfy the theoretical assumptions described above.

The combustion reaction products are another important element of the analysis. The model under consideration uses a two-stage global reaction. Therefore the products include CO, $CO_2$, $H_2O$, $SO_2$ and $NO_x$. Fig. 12 presents the carbon oxide mass fraction.

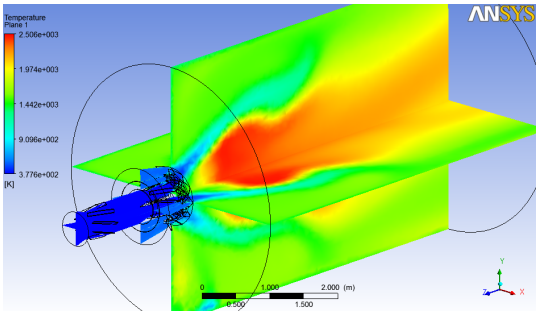


Figure 11: Temperature distribution [K] in the burner and in the furnace – isometric view of the ZY and ZX planes

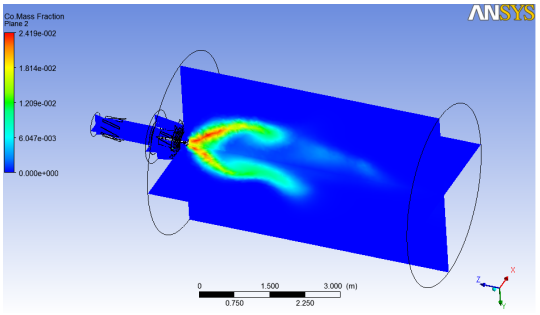


Figure 12: Carbon oxide mass fraction – isometric view of the YZ and YX planes

The maximum content of CO is 2.41%. The value seems relatively small, but this is a desirable phenomenon. The low content of combustible volatile fractions proves that combustion is nearly complete. The biggest concentration of carbon oxide occurs in the area above the flame, where the excess air factor drops below 0.7 and the mixture is oxygen-lean, which results in incomplete combustion. The content and shape of the carbon oxide particles presented on Fig. 12 are characteristic features of the sub-stoichiometric combustion zone formation. Fig. 13 shows the carbon dioxide mass fraction in flue gas. The maximum content in a given point does not exceed 33%. The biggest concentration of $CO_2$ occurs in the flame area, which is caused by the fact that carbon dioxide is produced in the reaction of carbon oxide created in the sub-stoichiometric zone with oxygen supplied from burner stage I and II (where it is burnt further).

Fig. 14 presents the oxygen mass fraction. In dark blue zones sub-stoichiometric combustion takes place with a shortage of the oxidant, which therefore is used completely. In the next zone, where the $\lambda$ value is higher than one, the oxygen is not fully used. The oxygen distribution indicates that the model operates according to the theoretical assumptions. The oxygen

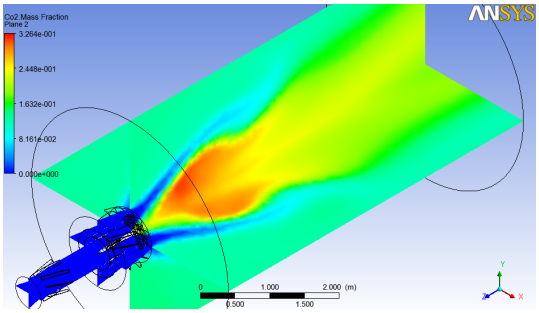


Figure 13: Carbon dioxide mass fraction – isometric view of the YZ and YX planes

mass fraction distribution is different compared to the model presented in [11], where a clear peak can be observed in the oxygen content close to the outlet and where no clear drop occurs in the oxygen content in the sub-stoichiometric zone. There is no such phenomenon in the case of the created CFD model, but a clearly visible zone of sub-stoichiometric combustion does appear. This may be caused by geometrical differences between the two burners or by different parameters of the coal dust or set boundary conditions.

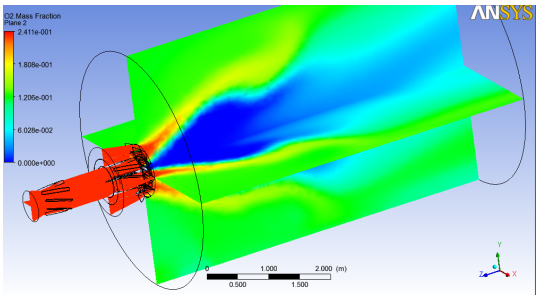


Figure 14: Oxygen mass fraction – isometric view of the YZ and YX planes

The picture below shows the sulfur dioxide mass fraction that is supplied to the combustion process in fuel only. Its dry ash free (DAF) content in the fuel does not exceed 1.4%, which results in low contents of sulfur oxides in flue gas – Fig. 15.

The last element of the calculated model analysis is the evaluation of burner operation effectiveness. Among other things, such burners are designed to minimize the emissions of harmful substances. In the post-processing stage, after incorporation of the $NO_x$ model, thermal and fuel oxides were taken into account. Fig. 16 presents the content of NO in the furnace.

The highest concentration of nitrogen oxides occurs directly at the burner outlet between the dust-air mixture and the stage II outlet. Then their content drops substantially. A similar dependence can be observed in [11].

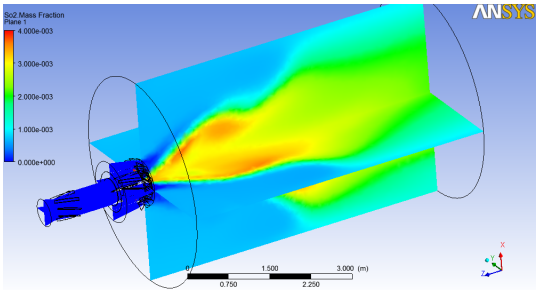


Figure 15: Sulfur dioxide mass fraction – isometric view of the YZ and YX planes

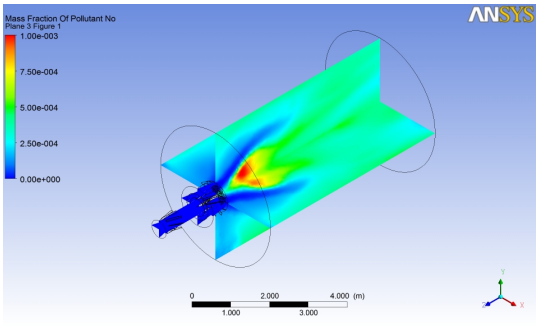


Figure 16: Mass fraction of nitrogen oxides – isometric view of the YZ and YX planes

## Conslusions

Based on the results, it can be concluded that the model developed operates correctly (i.e. its operation complies with the theoretical assumptions). The analysis also indicates that characteristic combustion zones with different excess air factors are formed in the furnace due to the swirling of the air and the coal dust mixture jets in individual stages of the swirlers.

The applied model of turbulence and turbulent combustion reflects the temperature in the furnace with fair accuracy, despite the fact that the model does not take into consideration: free radicals, dissociation effects or the soot combustion process. The PDF model should be used to improve accuracy, as it maps the conditions prevailing in the furnace better, without unduly inflating the temperature values [11]. However, in order to find a good compromise between the speed of computations and accuracy, the Eddy-Dissipation model seems to be sufficient. An improvement in the accuracy of results could also be achieved by iterating the model for greater conver-

gence or improving the mesh. This, however, would lengthen the time needed to perform the calculations. As a result of post-processing, the mass fractions of nitrogen oxides $NO_x$ were calculated. Their contents may be inflated slightly due to the fact that the Eddy-Dissipation model generally raises temperature. A rise in temperature involves increased formation of thermal nitrogen oxides. Nevertheless, the $NO_x$ content in flue gas seems to be satisfactory, which proves that the burner fulfils its role.

Generally, however, despite the fact that low-emission swirl coal dust burners bring some advantages, they are not widely used in industry. The situation is marginally better with swirl gas burners, as is reflected in the much greater number of available publications. Analyzing different examples of the use of low-emission swirl burners, it can be seen that such solutions offer many advantages. Despite their rather complex geometry compared to ordinary jet burners, low-emission swirl burners are economically justified because they cut emissions of undesirable gases, which translates into real financial savings. Another essential issue, which was signalled in the introduction, is the construction of the CFD model. Ansys software is used to map turbulent flows as accurately as possible without carrying out expensive experiments. The analysis presented herein leads to the conclusion that, despite some discrepancies between its results and those obtained in other studies and numerical calculations, it is possible to verify the model without having to build a prototype.

## References


1.Cho, C.H., Baek, G.M., Sohn, C.H., Cho, J.H., and Kim, H.S. (2013) A numerical approach to reduction of NOx emission from swirl premix burner in a gas turbine combustor. *Applied Thermal Engineering*, **59** (1-2), 454–463.

2.Holkar, R. (2013) CFD Anlysis of Pulverised-Coal Combustion of Burner Used In Furnace with Different Radiation Models. *IOSR Journal of Mechanical and Civil Engineering*, **5** (2), 25–34.

3.Dinesh, K.K.J.R., Luo, K.H., Kirkpatrick, M.P., and Malalasekera, W. (2013) Burning syngas in a high swirl burner: Effects of fuel composition. *International Journal of Hydrogen Energy*, **38** (21), 9028–9042.

4.GERMAN, A., and MAHMUD, T. (2005) Modelling of non-premixed swirl burner flows using a Reynolds-stress turbulence closure. *Fuel*, **84** (5), 583–594.

5.Hübner, A.W., Tummers, M.J., Hanjalić, K., and Meer, T.H. van der (2003) Experiments on a rotating-pipe swirl burner. *Experimental Thermal and Fluid Science*, **27** (4), 481–489.

6.Adamczyk, W.P., Werle, S., and Ryfa, A. (2014) Application of the computational method for predicting NO x reduction within large scale coal-fired boiler. *Applied Thermal Engineering*, **73** (1), 343–350.

7.Li, Z., Zeng, L., Zhao, G., Shen, S., and Zhang, F. (2011) Particle sticking behavior near the throat of a low-NOx axial-swirl coal burner. *Applied Energy*, **88** (3), 650–658.

8.Beckmann, A.M., Mancini, M., Weber, R., Seebold, S., and Müller, M. (2016) Measurements and CFD modeling of a pulverized coal flame with emphasis on ash deposition. *Fuel*, **167**, 168–179.

9.JAMALUDDIN, A.S., and SMITH, P.J. (1988) Predicting Radiative Transfer in Axisymmetric Cylindrical Enclosures Using the Discrete Ordinates Method. *Combustion Science and Technology*, **62** (4-6), 173–186.

10.Reis, L.C.B.S., Carvalho, J.A., Nascimento, M.A.R., Rodrigues, L.O., Dias, F.L.G., and Sobrinho, P.M. (2014) Numerical modeling of flow through an industrial burner orifice. *Applied Thermal Engineering*, **67** (1-2), 201–213.

11.Giorgi, M.G.D., Ficarella, A., and Laforgia, D. (2006) Optimization of an industrial coal pulverized swirled burner by CFD modelling. *61 Congresso Nazionale ATI, Perugia, Italy*.

12.KARDAŚ, D.A.R.I.U.S.Z., and GOLEC, S.L.A.W.O.M.I.R. (2005) Flow charateristics of a low NOx emission burner. *Task Quarterly*, **9** (1), 65–79.

13.Kurose, R., Makino, H., and Suzuki, A. (2004) Numerical analysis of pulverized coal combustion characteristics using advanced low-NOx burner. *Fuel*, **83** (6), 693–703.

14.Weber, R. (1996) Reaserch on low-emission combustion for industry furnaces. *Low-emission technics, Ustroń-Zawodzie, Poland*.

15.Zeldvich, Y.B. (1946) The oxidation of nitrogen in combustion and explosions. *J. Acta Physicochimica*, **21**, 577.

16.LAVOIE, G.E.O.R.G.E.A., HEYWOOD, J.O.H.N.B., and KECK, J.A.M.E.S.C. (1970) Experimental and Theoretical Study of Nitric Oxide Formation in Internal Combustion Engines. *Combustion Science and Technology*, **1** (4), 313–326.

17.Fenimore, C.P., and Jones, G.W. (1957) The Water-Catalyzed Oxidation of Carbon Monoxide by

Oxygen at High Temperature. *The Journal of Physical Chemistry*, **61** (5), 651–654.

18.Fenimore, C.P. (1971) Formation of nitric oxide in premixed hydrocarbon flames. *Symposium (International) on Combustion*, **13** (1), 373–380.